Composites Part B 218 (2021) 108935

Contents lists available at ScienceDirect

Composites Part B

journal homepage: www.elsevier.com/locate/compositesb

Fatigue damage tracking and life prediction of fiberglass composites using a laser induced graphene interlayer

LoriAnne Groo [a], Jalal Nasser [a], Daniel Inman [a], Henry Sodano [a,b,*]

[a] Department of Aerospace Engineering, University of Michigan, Ann Arbor, MI, 48109, USA
[b] Department of Materials Science and Engineering, University of Michigan, Ann Arbor, MI, 48109, USA

ARTICLE INFO

Keywords:
Laser induced graphene
Multifunctional composites
Fatigue life prediction
Piezoresistance
In-situ damage detection

ABSTRACT

Fiberglass-reinforced composite materials are commonly used in engineering structures subjected to dynamic loading, such as wind turbine blades, automobiles, and aircraft, where they experience a wide range of unpredictable operating conditions. The ability to monitor these structures while in operation and predict their remaining structural life without requiring their removal from service has the potential to drastically reduce maintenance costs and improve reliability. This work exploits piezoresistive laser induced graphene (LIG) integrated into fiberglass-reinforced composites for in-situ fatigue damage monitoring and lifespan prediction. The LIG is integrated within fiberglass composites using a transfer-printing process that is scalable with the potential for automation, thus reducing barriers for widespread application. The addition of the conductive LIG within the traditionally insulating fiberglass composites enables direct in-situ damage monitoring through simple passive resistance measurements during tension-tension fatigue loading. The accumulation and propagation of structural damage are detected throughout the fatigue life of the composite through changes to the electrical resistance measurements, and the measurement trends are further used to predict the onset of catastrophic composite failure. Thus, this work results in a scalable and multifunctional composite material with self-sensing capabilities for potential use in high-performing, dynamic, and flexible composite structures.

1. Introduction

Fiber-reinforced composite materials have been continuously replacing traditional homogeneous materials, particularly in streamlined, dynamic structures such as aircraft, small boats and automobiles. However, with the growing demand for high-performance structures comes additional desire for on-board structural monitoring systems that do not detrimentally affect the aerodynamic or mechanical performance of these composite materials. In addition, given the critical nature of these applications and the dynamic loading environments, there exists heightened interest in developing tools that are capable of anticipating the fatigue life of composite structures. However, such tasks are complicated by the anisotropy of fiber-reinforced composites, which causes them to be incompatible with commonly used traditional techniques for homogenous materials [1–3]. Therefore, to meet the demands for in-situ information regarding the damage state of various structures, structural health monitoring (SHM) for composite materials has been extensively researched and studied over the past several decades [4–8]. Concurrently, multiple researchers have investigated various empirical and phenomenological models for the purpose of fatigue life prognosis, specifically for fiber-reinforced composites [9,10]. Phenomenological models are commonly used to predict fatigue life in conjunction with SHM sensors that can provide actual in-situ information regarding the mechanical properties of the composites such as stiffness and strength [10–12]. For example, Suzuki et al. recently developed an improved model for fatigue life prediction for fiberglass composites based on stiffness degradation of the composites during loading [13]. The model was shown to be effective both for constant amplitude and random loading such as that experienced by fiberglass composites when exposed to ocean currents [13]. Nonetheless, in practice, this and other models require the development of in-situ SHM methods capable of monitoring the damage state of composite structures while in service. This acquisition of structural data in practice typically requires externally bonded sensors, which is impractical for large or complex structures due to the parasitic aerodynamic effects, environmental exposure, necessity for large systems of sensors, and difficulty in bonding to curved or complex surfaces. To reduce some of these limitations, alternative methods have turned to embedding of sensors such as lead zirconate titanate (PZT)

* Corresponding author. Department of Aerospace Engineering, University of Michigan, Ann Arbor, MI, 48109, USA.
E-mail address: hsodano@umich.edu (H. Sodano).

https://doi.org/10.1016/j.compositesb.2021.108935
Received 14 January 2021; Received in revised form 9 April 2021; Accepted 18 April 2021
Available online 21 April 2021

wafers [14,15], polyvinylidene fluoride (PVDF) films [16,17], or fiber optic sensors [18,19]. For example, Todd et al. utilized fiber Bragg grating sensors to detect fatigue damage in fiberglass composites and used the response of the sensor for composite life prognostics during fully reversed cyclic fatigue loading in a four-point bend configuration [20]. Although effective, these types of embedded sensors are still limited in application due to the weakening of the mechanical properties of the structures, as wafers and fluorinated films are introduced in the damage and failure-prone interlaminar areas of the composite, whereas optical fibers possess diameter size and properties that differ from those of the primary reinforcing fibers.

To meet the demands for aerodynamic composite structures, researchers have turned to the use of multifunctional composites that are capable of providing additional functionality, such as sensing or actuation, in addition to fulfilling their structural responsibilities. A well-researched example of this is the exploitation of the inherent piezoresistivity of carbon fibers for in-situ damage and strain monitoring [21–23]. As carbon fibers are strained, the molecular structure and the macroscopic shape of the material change, which results in modulation of the overall conductivity [24]. As the strain is increased to the point of mechanical failure of the fiber, sudden decreases in conductivity indicate fiber failure as a result of the reduced conductive pathways. Initially investigated in the late 1980s, resistance-based SHM for carbon fiber composites has been used to detect both strain and damage in multiple loading configurations, including tensile, flexural, impact, and fatigue [21,22,25–29]. In particular, changes in resistance to track damage progression during tension-tension fatigue have been examined by multiple research groups [30–32], where, in each case, the relative conductivity of the composite test specimen was shown to decrease proportional to the progress of fatigue life. In addition to using changes in the resistance of the carbon fiber composites to track damage, Seo et al. also demonstrated the potential for combining a pre-existing phenomenological model with trends in the electrical resistance to predict the fatigue damage incurred by the composite [30]. Vavouliotis et al. further extended these concepts by utilizing the trends in the resistance measurements to predict the fatigue life of the carbon fiber composite specimen [31]. Since the resistance of the sample was observed to decrease early during the fatigue test and then increase beyond a certain number of cycles, this inflection point was used to correlate the cycle at which the inflection occurs to the maximum number of cycles of the composite specimen [31]. However, despite the described research using scalable and effective methodology, it is limited to carbon fiber composites as it relies on the conductivity of the reinforcing fiber.

To extend resistance-based monitoring to composites reinforced with electrically insulating fibers, a significant amount of research has focused on using conductive nanomaterials, the most common of which is carbon nanotubes (CNTs) [33–36]. CNTs have grown in popularity within the field of multifunctional materials since embedding CNTs within fiber-reinforced composites results in improved mechanical properties as well as increased conductivity [37–39]. Taking advantage of their inherent conductivity, CNTs have been used for resistance-based monitoring of fiberglass-reinforced composites during tensile, impact, and flexural loading [33,40,41], in addition to tracking fatigue damage progression during tension-tension fatigue loading of fiberglass composites [42,43]. In particular, Böger et al. demonstrated that fiberglass composites with multi-wall CNTs (MWCNTs) showed an increasing electrical resistance measurement correlating to decreasing modulus during fatigue loading [43]. Furthermore, in addition to an increasing mean resistance value, the peak-to-peak value of the resistance during cyclic loading was also observed to increase during the test [43]. The referenced works conclusively demonstrate that fiberglass-reinforced composites with embedded CNTs exhibit changes in electrical resistance correlating to the damage progression of the host composites; however, the hybrid composites were only used to track damage progression and were not used to predict fatigue life. Additionally, dispersing CNTs within the matrix of fiber-reinforced composites requires careful processing techniques due to both the tendency of the CNTs to agglomerate due to van der Waals forces and the percolation requirements for effective resistance-based monitoring [44–46]. Efforts to circumvent these issues by depositing the CNTs directly onto the reinforcing fibers typically rely on chemical vapor deposition (CVD) or electrophoretic deposition (EPD), which either require extreme temperature and chemical environments or electrically conductive fibers, respectively [47–49]. To avoid the aforementioned problems, some research has investigated the use of CNTs in the form of buckypapers embedded within composites [50,51]. For example, Datta et al. utilized such a technique for fatigue monitoring and life prognosis of fiberglass composites [50]. However, the described methodology used only applied to crack propagation and was limited to single edge notch specimens. While small steps have been made to overcome issues associated with CNT fabrication, it stands to reason that alternative methodologies to introduce piezoresistive structural materials to fiberglass-reinforced composites would have the potential to improve the scalability and increase the application of resistance-based SHM for such materials.

As a more recent addition to the field of conductive carbon-based nanomaterials, laser induced graphene (LIG) has received extensive research attention because of the scalability and simplicity of the fabrication methods [52–54]. Initially introduced by Lin et al. [52], this method has since been used for toughening aramid- and carbon-fiber composite materials, while maintaining their tensile properties, or introduce multifunctionality in the form of strain and damage sensing in both aramid- and fiberglass-reinforced composites [55–58]. As a result of the polymeric makeup of aramid fibers, LIG can be directly generated by irradiating the surface fibers using a defocused CO_2 laser, thus leading to the direct conversion of the exposed fibers to piezoresistive LIG nanostructures [53,56,59,60]. The resultant multifunctional LIG-coated aramid composites are then capable of tracking tensile and flexural strain and damage [56], in addition to inter-ply delamination and ballistic impact [60]. However, since the chemical composition of ceramic fiberglass inhibits their direct conversion to LIG, a two-step transfer-printing process was developed to effectively integrate piezoresistive LIG within fiberglass prepreg composites, which are then capable of tracking tensile and flexural strain and damage [57]. Notably, prior work confirmed that the addition of the LIG within the inter-ply region of the composite had no impact on the composite cure, and was shown to result in maintained structural integrity as illustrated during short beam shear (SBS) testing and dynamic mechanical analysis (DMA) [57]. Furthermore, Nasser et al. investigated the optimization of the LIG transfer printing process for improved structural properties of composites fabricated with carbon fiber prepreg containing an LIG interlayer, and confirmed that the transfer printing of LIG to commercial prepregs does not affect the tensile loading properties of the prepreg [58].

This work further exploits the piezoresistivity of LIG for the tracking of damage during tension-tension fatigue loading through an electrical resistance-based monitoring approach. First, the LIG is embedded within commercial fiberglass prepregs using a transfer-printing process, thus enabling direct resistance measurements of the composite. The electrical resistance of each test specimen is then monitored throughout the duration of fatigue testing up until failure, and then compared against both the modulus of the composite specimen and strain measurements taken using digital image correlation (DIC). In addition to using the electrical resistance to track the progression of damage, the measurement statistics are also shown to allow for the prediction of the remaining fatigue life. The composite fabrication methods used here are scalable and economical as the LIG is printed onto the surface of commercial polyimide films, and then transferred to commercial fiberglass prepreg. Notably, these processes avoid the need for any complex pretreatment or chemical surface modifications. Thus, this work introduces a novel material with the potential to overcome current

limitations inhibiting the widespread application of resistance-based monitoring for fatigue life monitoring and prediction in fiberglass-reinforced composites.

2. Materials and methods

2.1. LIG fabrication and composite layup

In this work, a simple transfer-printing process was used to integrate LIG within fiberglass composites. For reference, this methodology is more fully detailed and characterized elsewhere [57]. In short, a commercial polyimide film (0.0254 mm thick Kapton® tape sheets) was irradiated using a 40 W CO_2 infrared laser (Epilog Zing 16). Following the conversion of the polyimide to LIG, the LIG interlayer was transferred to the surface of an uncured fiberglass prepreg (CYCOM® E773) through a transfer printing process that consists of rolling the prepreg onto the LIG-coated polyimide substrate while applying manual pressure. The LIG was thus embedded in the uncured prepreg, forming an interlayer, after which the fiberglass prepreg layers were combined in a [+45/-45/+45]° stacking sequence and cured in a hot press at 127 °C under 100 psi (689.5 kPa) for 2 h. Once the composite panel was cured, samples were cut to 10 mm in width and 76 mm in length for quasi-static tensile testing to failure and tension-tension fatigue testing. Fiberglass tabs were then attached to each end of the sample with high shear strength epoxy (Loctite® 9430™ Hysol®) before adding sandpaper to the outside of the fiberglass tabs to eliminate slipping during the testing. The final gauge length of the samples following tab attachment was approximately 35 mm. To enable resistance measurements of the composite samples during testing, thin lines of silver paint were added around the edge of the sample at each end, resulting in a conductive pathway between each ply. Consequently, the resistance measurements taken between each silver paint ring were those of the entire composite rather than just the LIG interlayer at the surface ply. Additionally, copper wires were attached to the silver paint rings using additional silver paint and quick-cure epoxy to keep the wires fixed during testing. For reference, the electrical resistance of the samples following the completion of the fabrication process ranged between 200 and 900 Ω. Finally, white spray paint was used to speckle the top LIG-coated surface of the sample for DIC measurements. For reference, a side-view schematic of the sample with the direction of the applied load is shown in Fig. 1a, an image of the composite cross-section taken using an optical microscope is shown in Fig. 1b, and an image of a portion of the composite cross-section taken using a scanning electron microscope (SEM) is shown in Fig. 1c.

2.2. Fatigue testing

The completed test specimens were first evaluated in a quasi-static tensile test to failure using an Instron model 5982 test frame with a 100 kN load cell according to ASTM standard D3039. Seven samples from multiple composite panels were tested to determine the average ultimate stress of the LIG-coated fiberglass composites ($\sigma_{ultimate}$). Following the testing to failure, ten additional samples were tested in a load-controlled tension-tension fatigue test using an Instron ElectroPuls™ model E1000 test frame with a ±1 kN load cell. A sine wave excitation was used at a 10 Hz frequency and an R-value of 0.1, where R is defined as the ratio between the minimum stress and the maximum stress during the loading cycle ($R = \sigma_{min}/\sigma_{max}$). In order to obtain the response of the LIG over a small range of applied loads and fatigue life duration, the samples were subjected to a maximum stress (σ_{max}) ranging between 65 and 78% of the ultimate strength ($\sigma_{ultimate}$). While the elastic stiffness of the samples was monitored by the test frame, images for DIC analysis were taken using a single high speed camera (Photron FASTCAM Mini AX 200 high-speed camera) placed 125 mm from the sample with a field of view approximately 14 mm wide and 28 mm long. Periodically throughout the tests (every 500–1000) cycles, 100 frames were collected at 1000 frames per second (FPS) which covers one full cycle as the samples were loaded at 10 Hz. The DIC analysis and correlating surface strain measurements were performed using Vic-2D software [61], and the mean strain measured along the loading direction averaged across the full sample width and 26 mm of the sample length was reported. It can be noted that 26 mm in length was used rather than 28 mm due to the focus of the camera. For reference, the strain halfway through the sinusoidal loading cycle was used. The electrical resistance of each sample was concurrently monitored using a Wheatstone bridge through the test, where the circuit input was provided by a DC power supply (Hewlett Packard model 6217A) and the output was recorded using a National Instruments (NI) compact data acquisition system (cDAQ 9174) with an NI-9223 input module. A schematic of the fatigue test setup is shown in Fig. 2.

3. Results and discussion

3.1. Fatigue testing results

Throughout the fatigue testing, the elastic modulus of the specimens was measured by the load frame, while the accumulation of damage in the sample was monitored through DIC measurements. To provide a more direct comparison between samples, the calculated values for the modulus and strain were normalized by their respective values at the

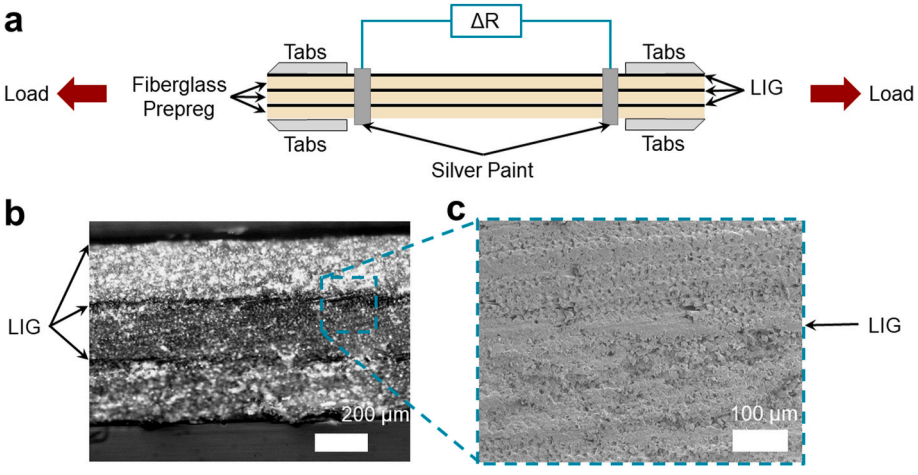

Fig. 1. (a) Side-view schematic of the prepared sample and the direction of the applied load. (b) Image of the composite cross-section taken using an optical microscope. (c) Image of a portion of the composite cross-section taken using a SEM.

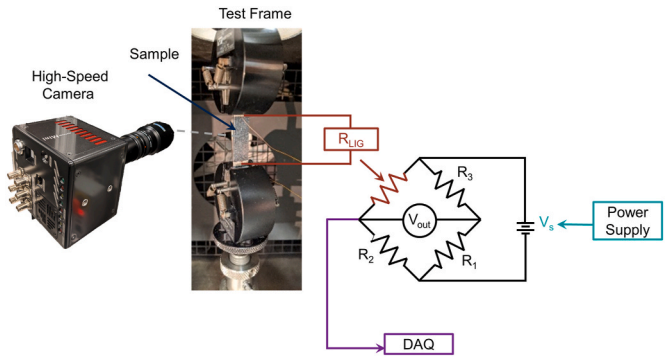

Fig. 2. Schematic of fatigue sample in test frame with setup for in-situ resistance monitoring and DIC analysis.

beginning of the first loading cycle. Additionally, the normalized fatigue life of each sample was determined by normalizing the cycles during each test by the corresponding number of cycles to failure for each sample. The normalized decrease in the elastic modulus versus the normalized fatigue life for each sample is shown in Fig. 3a. As expected, the observed trends in decreasing stiffness allow for the categorization of the fatigue tests into three main regions. The literature has defined these regions by the type of damage initiation and propagation predominantly experienced by the sample during those portions of the fatigue life [31, 62]. In Region I (approximately $<$ 15% of fatigue life), the sample failure is dominated by matrix cracking throughout the composite. Since the samples tested here consist of entirely off-axis plies, the matrix cracking occurs in each ply and results in a relatively high rate of increase in the average strain experienced by the sample during this region [62]. This can also be confirmed by the DIC measurements shown in Fig. 3b, which indicate a sharp increase in strain during the same portion of the test. Region II (approximately 15–85% of fatigue life) is characterized by interfacial debonding occurring within the interlaminar area of the composite, delamination occurring along the off-axis fibers, additional matrix cracking, and the propagation of all these types of damage. During this portion of the test, both the decrease in modulus and the measured strain show relatively linear increases at a lower rate than that observed in Region I or III, which is characteristic of the damage propagation in Region II [62]. Finally, Region III (approximately $>$ 85% of fatigue life) occurs toward the end of the test and immediately preceding failure of the composite. This portion of the test is characterized by severe fiber fracture and pullout combined with a large degree of delamination along the fiber direction, both of which result in the dramatic decrease in modulus and increase in strain observed in Fig. 3a and b, respectively. It can be therefore noted that the trends observed here are similar to those observed in previous studies reported in the literature [62–64].

In addition to monitoring the structural changes using the modulus and strain measurements, the electrical resistance of the samples was also measured throughout the duration of the test to evaluate the self-sensing capabilities of the composites containing LIG. As the samples were cyclically loaded at 10 Hz, the resistance measurements were averaged to obtain one representative measurement each second, resulting in one measurement point for every 10 cycles. The resistance measurements were then normalized by the mean resistance value measured during the first second of the test in order to enable accurate comparison between samples. The resulting average percent change in the mean resistance (ΔR) for each sample versus the normalized fatigue life is shown in Fig. 4. The trends in the normalized ΔR also show some correlation to the three regions characterized by the type of damage occurring within the fiberglass samples. Since the piezoresistive LIG is located within the matrix at each ply level, multiple damage types including matrix cracking, delamination, and fiber breakage are all detectable by the changes in electrical resistance due to the resulting physical separations within the LIG interlayer [57]. However, the increase in ΔR experienced during matrix cracking, which occurs during Region I, is considerably less pronounced than the increase observed during debonding, delamination, and fiber failure which occur during Regions II and III. This can be explained by the fact that matrix cracking results in less physical separation within the LIG interlayer, and therefore it is less likely to significantly affect the electrical conductivity. Nonetheless, the percent change in the mean resistance can be used to track the progression of fatigue damage within the composite samples throughout each region of the fatigue life.

In addition to relying on the ΔR to evaluate the progression of damage within the fiberglass composites samples, the first derivative of the normalized resistance taken with respect to the number of cycles provides further insight into the mechanisms at play in the increasing resistance measurements. Fig. 5 shows the first derivative of the normalized percent change in resistance taken with respect to the number of cycles in log-scale versus the normalized fatigue life. It should be noted that the results shown in Fig. 5 are not a direct derivative of those shown in Fig. 4, and are instead the derivative of the normalized resistance measurements with respect to cycles during the test rather than the normalized fatigue life. It should be noted that in practice, where the fatigue life of the composite is unknown, the number of cycles experienced by the composite can be tracked using the time response of

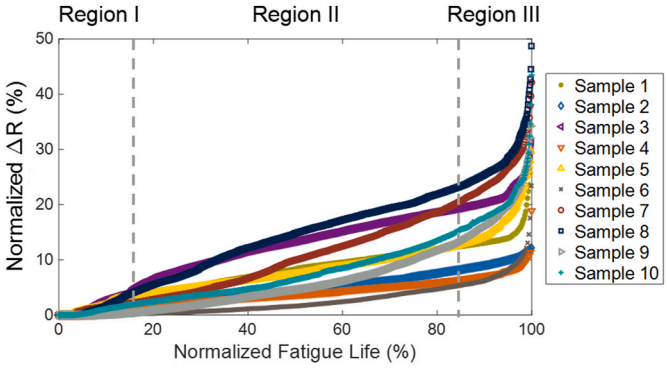

Fig. 4. Normalized ΔR versus normalized fatigue life.

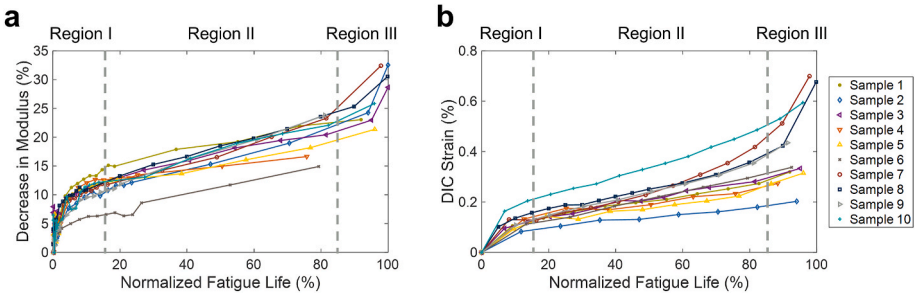

Fig. 3. (a) Decrease in modulus versus normalized fatigue life. (b) Strain from DIC measurements versus normalized fatigue life.

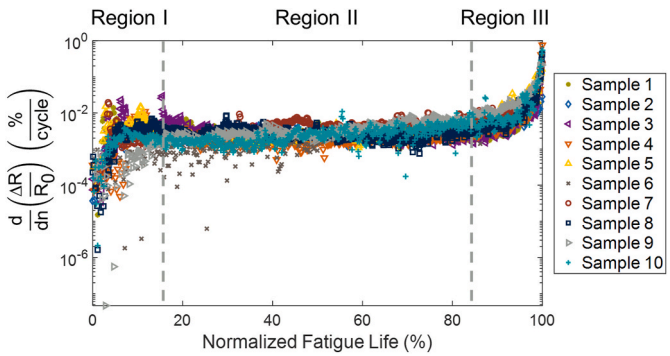

Fig. 5. Derivative of normalized change in resistance versus normalized fatigue life.

the resistance. In this case, since a sinusoidal loading wave was used, the time response of the sample resistance also followed a sinusoidal pattern. Thus, the measured resistance from the sample can be used to determine the number of cycles without requiring knowledge of the load. It is apparent from the results in Fig. 5 that the same three regions defined by the physical effects of the damage within the composite samples are also clearly detectable by the variation in the slope of the first derivative of the normalized electrical resistance throughout the normalized fatigue life. Initially during Region I, where matrix cracking is the dominant damage form, the normalized resistance (Fig. 4) increases at a relatively low rate resulting in a lower derivative (Fig. 5). This is due to the location of the LIG within the matrix of the composite. Thus, as the matrix is damaged, a relatively small amount of corresponding separation occurs within the LIG. Then, as delamination, debonding, additional matrix cracking, and some small fiber damage occur, the resistance increases approximately linearly, which results in a constant derivative. During Region III, however, the fiber breakage and severe delamination result in significant physical separation between conductive contacts within the LIG interlayers, leading to a non-linear increase in electrical resistance, which correlates to the non-linear physical effects (Fig. 3). The described trends are notably consistent regardless of the initial specimen resistance or applied stress, thus yielding the good alignment observed in Fig. 5. As a result of the consistency in the trends observed from each sample and the distinctive Regions I, II, and III, the derivative of the normalized resistance with respect to cycles is a promising candidate for fatigue life prediction, which will be further discussed in a later section.

To provide a visual comparison between the three measurement methods, the normalized ΔR, decrease in modulus, and physical damage observed using DIC measurements for a representative sample (Sample 8) are shown in Fig. 6a and Fig. 6b. The images corresponding to the DIC measurements (Fig. 6b) represent the strain in the loading direction (ε_{yy}), which is 45° off-axis from the fiber orientation of each ply. The combined data in Fig. 6 further validates the conclusions drawn regarding the damage detected during each region of testing. While the matrix cracking in Region I results in a slight decrease in modulus and visual increase in strain, the increase in ΔR and decrease in modulus become approximately linear when damage progresses through Region II, as some delamination along the fibers is visible in the DIC images. Then, in Region III at the end of the test (>85% fatigue life), the non-linear increase in ΔR is visually correlated to fiber breakage and severe delamination, highlighted by the highly concentrated areas of damage in the DIC images, as the sample fails in shear due to the stacking sequence of the plies. For additional confirmation of the correlation between the changes in normalized ΔR and the strain measured by the DIC, a comparison of the normalized ΔR and DIC strain for three representative samples is shown in Fig. 6c. From the figure, the trend in ΔR is shown to correlate well to the trends in the measured strain due to the piezoresistivity of the LIG. This correlation improves as the test

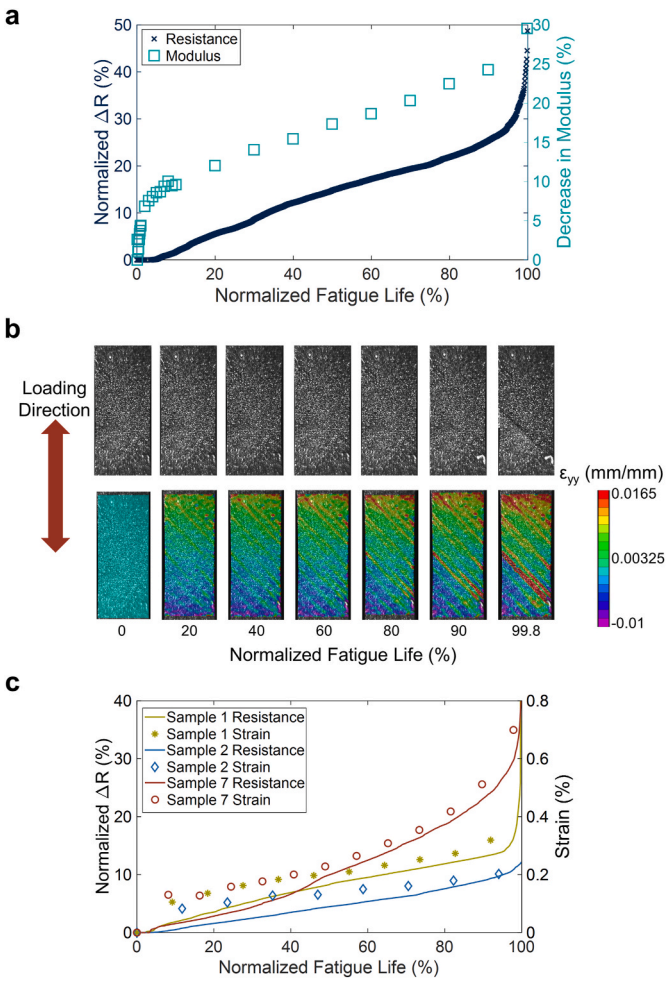

Fig. 6. (a) Normalized ΔR and decrease in modulus versus normalized fatigue life. (b) High speed camera photos of a sample and corresponding DIC images of strain in the loading direction (ε_{yy}) versus normalized fatigue life (c) Normalized ΔR and DIC strain versus normalized fatigue life.

progresses through Region II and III as the fatigue life is between ~40 and 100%. This is expected based on prior works which have investigated the ability of LIG to track strain in fiberglass-reinforced composites through resistance measurements [57].

In addition to monitoring the mean resistance measurements (ΔR), the peak-to-peak value of the resistance (ΔR_{pp}) was also used to track trends in the structural damage to the composite during fatigue loading. In contrast to ΔR, the values of ΔR_{pp} represent the maximum peak-to-peak value over 1 s of data. As a result, the measurements were highly susceptible to environmental noise, and a post-processing filter was used to reduce the high-frequency noise and eliminate the data points corresponding to high levels of noise. It should also be noted that ΔR_{pp} measurements were normalized by the initial value of R_{pp} during the first second of data to again provide a fair comparison between samples. Since the tests were performed in a load-control mode, the specimens exhibited larger strains as testing progressed while the elastic modulus decreased due to the accumulated damage. This expected increase in peak-to-peak strain values in return led to increased ΔR_{pp} as a direct consequence of the piezoresistance of the LIG. It can also be noted that a similar increasing trend in ΔR_{pp} of fiberglass composites containing CNTs has also been reported in the literature [43]. The resulting normalized changes in ΔR_{pp} versus the normalized fatigue life for each sample tested are shown in Fig. 7. The results presented in the figure indicate that ΔR_{pp} increasess approximately linearly until the sample approach Region III of failure. As the samples near failure in Region III,

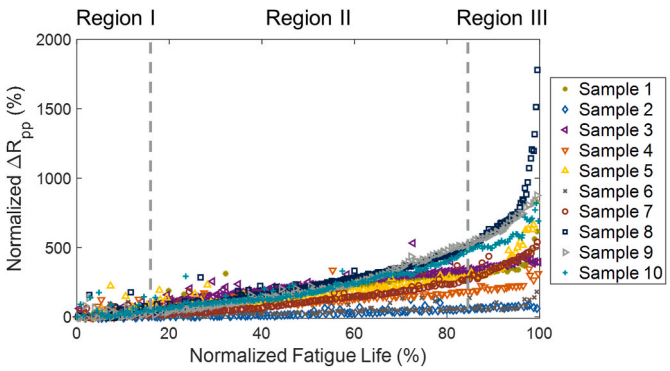

Fig. 7. Normalized ΔR_{pp} versus normalized fatigue life.

the moduli change non-linearly, and ΔR_{pp} measurements show a similar trend due to the severe damage experienced by the composite samples in this region. The relatively linear behavior through Region I is attributed to the fact that in that region, the minor changes in specimen modulus do not cause sufficiently large alterations in the slope of the peak-to-peak strain, which in return minimizes changes within ΔR_{pp}. The response in Region II is linear as expected because changes in the modulus, strain, and ΔR are observed to be approximately linear here. This linearity is due to the relatively constant increase in damage modes experienced in this region. In summary, ΔR_{pp} is promising for the estimation of fatigue life due to the consistently linear increase in the normalized value during Region I of the fatigue life.

3.2. Fatigue life prediction

Further analysis of the ΔR_{pp} measurements indicates that a certain degree of correlation exists between the rate of increase in ΔR_{pp} and the fatigue life of the fiberglass composite. To take advantage of the proportional relationship between the resistance and strain measurements, a linear fit was applied to ΔR_{pp} versus the cycles during the first portion of the test (0–2000 cycles). The normalized experimental peak-to-peak data and the corresponding linear fit for the first 2000 cycles are shown in Fig. 8a for a representative sample (Sample 3). The cycle range selected correlates to the data up to 20–50% of the fatigue life for the samples tested in this work. In order for fatigue life prediction to be maximally effective, it is desirable that the estimation be made early during the life of the composite prior to the occurrence of significant damage to the composite material. Thus, a limit of 2000 cycles was selected here, as it is the minimum number of cycles covering Region I of failure for the all the tested samples. Although this number includes the first portion of Region II for some samples, the linear trend in the peak-to-peak resistance is observed to persist through Region I and into Region II (Fig. 7). Once the linear fit was applied to the first 2000 cycles of each sample, the maximum number of cycles was plotted versus the slope of these linear fits for each sample (Fig. 8b). From the figure, the fatigue life of the sample is shown to increase approximately linearly with the slope of the normalized ΔR_{pp}. A least squares linear fit of the trend seen in Fig. 8b results in a good correlation with the experimental data, as the majority of test specimens fall within one standard deviation of the fit. Therefore, the results indicate that the slope of the normalized ΔR_{pp} versus the cycle number within Region I and the early part of Region II during the fatigue life is a promising approach for obtaining an initial estimation of the predicted fatigue life of the test specimen without requiring knowledge of the applied load.

Although the normalized ΔR_{pp} can provide some indication of the sample fatigue life, additional information regarding the progression towards structural failure is still desirable during unpredictable, dynamic loading environments. For this reason, additional analysis was completed for the derivative of the normalized resistance measurements. As previously stated, the trends in the derivative showed good correlation for each sample tested during the entirety of the fatigue life, regardless of the applied load or induced strain. Fig. 5 illustrated that each sample showed a relatively constant derivative during Region II with a slight increase, followed by a non-linear increase as the sample approaches failure in Region III. Thus, the observed trends from Region II and Region III show a close correlation with an exponential curve. In order to further exploit this relationship, the derivatives of the samples were averaged over the normalized fatigue life, and a non-linear least-squares curve fit was applied to obtain a model exponential curve correlating to the relationship between the $\log_{10}$ of the mean derivative and the sample fatigue life. It is interesting to note that while this method, which uses the derivative of the resistance, models the relationship between the entirety of the data set and the fatigue life, the prior method using ΔR_{pp} utilizes only a single data point representing each sample to obtain the predicted fatigue life. The experimental first derivative corresponding to the entire sample set, calculated average of the sample derivatives, and the resultant exponential fit are shown in Fig. 9. From the figure, the exponential curve shows excellent correlation with the mean derivative and good correlation to the bulk of the

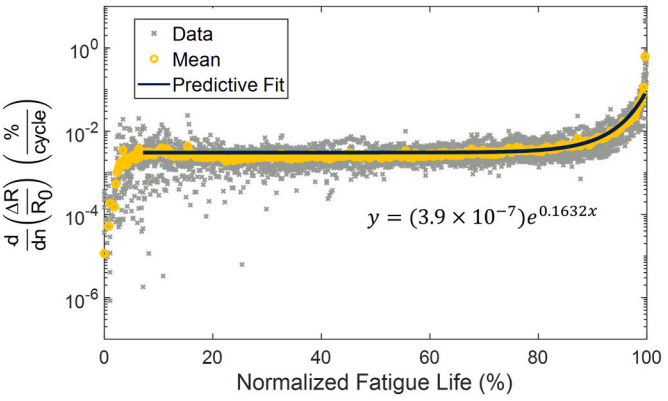

Fig. 9. Derivative of normalized change in resistance versus normalized fatigue life with exponential predictive fit.

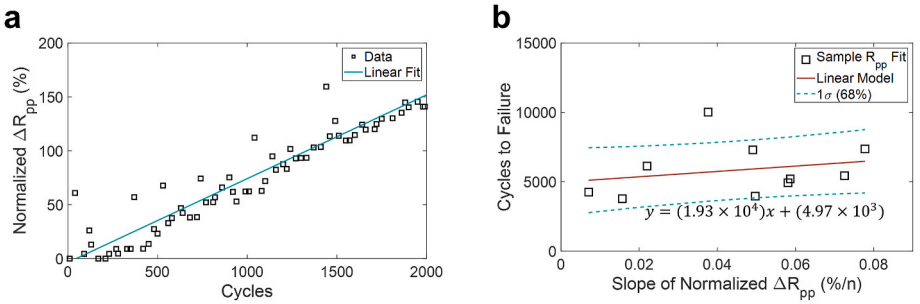

Fig. 8. (a) Sample 3 normalized ΔR_{pp} versus cycles with a linear fit. (b) Fatigue life versus slope of normalized ΔR_{pp} with a linear fit.

experimental data from all samples tested. The results thus indicate the derivative of the normalized resistance measurements with respect to cycles can be correlated to the fatigue life of the sample with no knowledge of the loading amplitude or fatigue life. Although there is some variation in the derivatives early on during the test (<20% normalized fatigue life), ΔR_{pp} can be used to provide an initial estimation of the fatigue life during Region I, while the derivatives can be used to provide a more accurate fatigue life estimation as the sample progresses towards failure in Regions II and III. It can be noted that in future work, both phenomenological models and machine learning algorithms, such as artificial neural networks (ANNs), will be investigated as potential approaches for more accurately predicting the remaining fatigue life and future damage state of composite materials using the piezoresistive response of the embedded LIG interlayers. It is also recommended that future work investigate the use of the methodology used here for truly random loading environments which lack constant load frequency and amplitude.

4. Conclusion

This work exploits piezoresistive LIG for fatigue damage tracking and fatigue life estimation in fiberglass-reinforced composites. First, LIG is integrated within fiberglass composites using a scalable transfer-printing process, after which the composite samples are subjected to tension-tension fatigue loading while monitoring the stiffness, strain, average electrical resistance, and peak-to-peak electrical resistance. The results indicate that the normalized resistance measurements and peak-to-peak resistance measurements can be used to track matrix cracking, delamination, and fiber failure within the loaded fiberglass composites. Additionally, the peak-to-peak measurements were shown to increase approximately linearly with the number of cycles, and the corresponding slope was shown to have an approximately linear relationship with the overall fatigue life of the sample. The slope of the peak-to-peak measurements can therefore be used to estimate the fatigue life during Region I of the composite fatigue damage. Furthermore, an exponential model is used to correlate the derivative of the normalized resistance measurements to the fatigue life as the samples approach fatigue failure (>75% of normalized fatigue life). Thus, for the first time, piezoresistive LIG is used for both damage tracking and fatigue life estimation in fiberglass composites exposed to cyclic sinusoidal loading. Although further investigation is recommended for random or unpredictable dynamic loading environments, these preliminary results indicate that this novel multifunctional material has potential for use in SHM and fatigue life prediction applications. Future work will explore the potential of combining such an SHM technique with machine learning algorithms to provide accurate fatigue life prediction under unknown and unpredictable loading conditions.

CRediT authorship contribution statement

LoriAnne Groo: Conceptualization, Investigation, Writing – original draft. **Jalal Nasser:** Conceptualization, Investigation, Writing – original draft. **Daniel Inman:** Project administration, Methodology, Writing – review & editing, Funding acquisition. **Henry Sodano:** Conceptualization, Project administration, Methodology, Funding acquisition, Supervision, Writing – review & editing.

Declaration of competing interest

The authors declare that they have no known competing financial interests or personal relationships that could have appeared to influence the work reported in this paper.

Acknowledgements

The authors gratefully acknowledge support from the National Science Foundation Graduate Research Fellowship Program [grant number DGE 1256260]; National Science Foundation [grant numbers CMMI-1762369, EFRI-1935216]; and the Air Force Office of Scientific Research [grant number FA9550-16-1-0087].

References

[1] Seale MD, Smith BT, Prosser W, Zalameda JN. Lamb wave assessment of fiber volume fraction in composites. J Acoust Soc Am 1998;104(3):1399–403.
[2] Surgeon M, Wevers M. Modal analysis of acoustic emission signals from CFRP laminates. NDT E Int 1999;32(6):311–22.
[3] Mechraoui S-E, Laksimi A, Benmedakhene S. Reliability of damage mechanism localisation by acoustic emission on glass/epoxy composite material plate. Compos Struct 2012;94(5):1483–94.
[4] Sohn H, Farrar CR, Hemez FM, Shunk DD, Stinemates DW, Nadler BR, et al. A review of structural health monitoring literature: 1996–2001. USA: Los Alamos National Laboratory; 2003. p. 1.
[5] Giurgiutiu V, Zagrai A, Bao J. Damage identification in aging aircraft structures with piezoelectric wafer active sensors. J Intell Mater Syst Struct 2004;15(9–10):673–87.
[6] Zhao X, Gao H, Zhang G, Ayhan B, Yan F, Kwan C, et al. Active health monitoring of an aircraft wing with embedded piezoelectric sensor/actuator network: I. Defect detection, localization and growth monitoring. Smart Mater Struct 2007;16(4):1208–17.
[7] Yang J, Chang F-K. Detection of bolt loosening in C–C composite thermal protection panels: I. Diagnostic principle. Smart Mater Struct 2006;15(2):581–90.
[8] Montalvao D, Maia NMM, Ribeiro AMR. A review of vibration-based structural health monitoring with special emphasis on composite materials. Shock Vib Digest 2006;38(4):295–324.
[9] Post NL, Case SW, Lesko JJ. Modeling the variable amplitude fatigue of composite materials: a review and evaluation of the state of the art for spectrum loading. Int J Fatig 2008;30(12):2064–86.
[10] Shiri S, Yazdani M, Pourgol-Mohammad M. A fatigue damage accumulation model based on stiffness degradation of composite materials. Mater Des 2015;88:1290–5.
[11] Zhang C, Zhang Z, Ji H, Qiu J, Tao C. Mode conversion behavior of guided wave in glass fiber reinforced polymer with fatigue damage accumulation. Compos Sci Technol 2020;192:108073.
[12] Peng T, Liu Y, Saxena A, Goebel K. In-situ fatigue life prognosis for composite laminates based on stiffness degradation. Compos Struct 2015;132:155–65.
[13] Suzuki T, Mahfuz H, Takanashi M. A new stiffness degradation model for fatigue life prediction of GFRPs under random loading. Int J Fatig 2019;119:220–8.
[14] Tang H-Y, Winkelmann C, Lestari W, La Saponara V. Composite structural health monitoring through use of embedded PZT sensors. J Intell Mater Syst Struct 2011;22(8):739–55.
[15] Giurgiutiu V, Zagrai A, Bao J. Embedded active sensors for in-situ structural health monitoring of thin-wall structures. J Pressure Vessel Technol 2002;124(3):293–302.
[16] De Rosa IM, Sarasini F. Use of PVDF as acoustic emission sensor for in situ monitoring of mechanical behaviour of glass/epoxy laminates. Polym Test 2010;29(6):749–58.
[17] Caneva C, De Rosa I, Sarasini F. Damage mechanisms in loaded aramid composites by means of embedded PVDF acoustic emission sensors. Advanced materials research. Trans Tech Publ; 2006. p. 337–42.
[18] Read I, Foote P, Murray S. Optical fibre acoustic emission sensor for damage detection in carbon fibre composite structures. Meas Sci Technol 2001;13(1):N5–9.
[19] Wu Q, Yu F, Okabe Y, Kobayashi S. Application of a novel optical fiber sensor to detection of acoustic emissions by various damages in CFRP laminates. Smart Mater Struct 2014;24(1):015011.
[20] Todd M, Gregory W, Key C, Yeager M, Ye J. Composite laminate fatigue damage detection and prognosis using embedded fiber Bragg gratings. ASME 2018 conference on smart materials, adaptive structures and intelligent systems. American Society of Mechanical Engineers Digital Collection; 2018.
[21] Baron C, Schulte K. Determination of electric resistance for in situ determination of fibre failure in carbon fibre-reinforced plastic composites. Material-pruefung. 1988;30(11–12):361–6.
[22] Schulte K, Baron C. Load and failure analyses of CFRP laminates by means of electrical resistivity measurements. Compos Sci Technol 1989;36(1):63–76.
[23] Chung DDL. Self-monitoring structural materials. Mater Sci Eng R Rep 1998;22(2):57–78.
[24] Blazewicz S, Patalita B, Touzain P. Study of piezoresistance effect in carbon fibers. Carbon 1997;35(10):1613–8.
[25] Wang X, Fu X, Chung DDL. Strain sensing using carbon fiber. J Mater Res 2011;14(3):790–802.
[26] Abry JC, Bochard S, Chateauminois A, Salvia M, Giraud G. In situ detection of damage in CFRP laminates by electrical resistance measurements. Compos Sci Technol 1999;59(6):925–35.
[27] Wang S, Chung D. Self-sensing of flexural strain and damage in carbon fiber polymer-matrix composite by electrical resistance measurement. Carbon 2006;44(13):2739–51.
[28] Wang S, Chung DDL, Chung JH. Impact damage of carbon fiber polymer–matrix composites, studied by electrical resistance measurement. Compos Appl Sci Manuf 2005;36(12):1707–15.

[29] Wen J, Xia Z, Choy F. Damage detection of carbon fiber reinforced polymer composites via electrical resistance measurement. Compos B Eng 2011;42(1):77–86.
[30] Seo D-C, Lee J-J. Damage detection of CFRP laminates using electrical resistance measurement and neural network. Compos Struct 1999;47(1–4):525–30.
[31] Vavouliotis A, Paipetis A, Kostopoulos V. On the fatigue life prediction of CFRP laminates using the Electrical Resistance Change method. Compos Sci Technol 2011;71(5):630–42.
[32] Wang X, Chung DDL. Self-monitoring of fatigue damage and dynamic strain in carbon fiber polymer-matrix composite. Compos B Eng 1998;29(1):63–73.
[33] Gao L, Thostenson ET, Zhang Z, Chou T-W. Sensing of damage mechanisms in fiber-reinforced composites under cyclic loading using carbon nanotubes. Adv Funct Mater 2009;19(1):123–30.
[34] Gao Sl, Zhuang RC, Zhang J, Liu JW, Mäder E. Glass fibers with carbon nanotube networks as multifunctional sensors. Adv Funct Mater 2010;20(12):1885–93.
[35] Gallo GJ, Thostenson ET. Spatial damage detection in electrically anisotropic fiber-reinforced composites using carbon nanotube networks. Compos Struct 2016;141:14–23.
[36] Baltopoulos A, Polydorides N, Pambaguian L, Vavouliotis A, Kostopoulos V. Exploiting carbon nanotube networks for damage assessment of fiber reinforced composites. Compos B Eng 2015;76:149–58.
[37] Khan SU, Li CY, Siddiqui NA, Kim J-K. Vibration damping characteristics of carbon fiber-reinforced composites containing multi-walled carbon nanotubes. Compos Sci Technol 2011;71(12):1486–94.
[38] Jang J-S, Varischetti J, Suhr J. Strain dependent energy dissipation in multi-scale carbon fiber composites containing carbon nanofibers. Carbon 2012;50(11):4277–83.
[39] Thostenson E, Li W, Wang D, Ren Z, Chou T. Carbon nanotube/carbon fiber hybrid multiscale composites. J Appl Phys 2002;91(9):6034–7.
[40] Alexopoulos ND, Bartholome C, Poulin P, Marioli-Riga Z. Structural health monitoring of glass fiber reinforced composites using embedded carbon nanotube (CNT) fibers. Compos Sci Technol 2010;70(2):260–71.
[41] Arronche L, La Saponara V, Yesil S, Bayram G. Impact damage sensing of multiscale composites through epoxy matrix containing carbon nanotubes. J Appl Polym Sci 2013;128(5):2797–806.
[42] Nofar M, Hoa SV, Pugh MD. Failure detection and monitoring in polymer matrix composites subjected to static and dynamic loads using carbon nanotube networks. Compos Sci Technol 2009;69(10):1599–606.
[43] Böger L, Wichmann MH, Meyer LO, Schulte K. Load and health monitoring in glass fibre reinforced composites with an electrically conductive nanocomposite epoxy matrix. Compos Sci Technol 2008;68(7–8):1886–94.
[44] Parmar K, Mahmoodi M, Park C, Park SS. Effect of CNT alignment on the strain sensing capability of carbon nanotube composites. Smart Mater Struct 2013;22(7):075006.
[45] Tehrani M, Boroujeni A, Hartman T, Haugh T, Case S, Al-Haik M. Mechanical characterization and impact damage assessment of a woven carbon fiber reinforced carbon nanotube–epoxy composite. Compos Sci Technol 2013;75:42–8.
[46] Gojny F, Wichmann M, Köpke U, Fiedler B, Schulte K. Carbon nanotube-reinforced epoxy-composites: enhanced stiffness and fracture toughness at low nanotube content. Compos Sci Technol 2004;64(15):2363–71.
[47] Zhang Q, Liu J, Sager R, Dai L, Baur J. Hierarchical composites of carbon nanotubes on carbon fiber: influence of growth condition on fiber tensile properties. Compos Sci Technol 2009;69(5):594–601.
[48] An Q, Rider AN, Thostenson ET. Electrophoretic deposition of carbon nanotubes onto carbon-fiber fabric for production of carbon/epoxy composites with improved mechanical properties. Carbon 2012;50(11):4130–43.
[49] Bekyarova E, Thostenson E, Yu A, Kim H, Gao J, Tang J, et al. Multiscale carbon nanotube− carbon fiber reinforcement for advanced epoxy composites. Langmuir 2007;23(7):3970–4.
[50] Datta S, Neerukatti RK, Chattopadhyay A. Buckypaper embedded self-sensing composite for real-time fatigue damage diagnosis and prognosis. Carbon 2018;139:353–60.
[51] Zhang Z, Wei H, Liu Y, Leng J. Self-sensing properties of smart composite based on embedded buckypaper layer. Struct Health Monit 2015;14(2):127–36.
[52] Lin J, Peng Z, Liu Y, Ruiz-Zepeda F, Ye R, Samuel EL, et al. Laser-induced porous graphene films from commercial polymers. Nat Commun 2014;5:5714.
[53] Chyan Y, Ye R, Li Y, Singh SP, Arnusch CJ, Tour JM. Laser-induced graphene by multiple lasing: toward electronics on cloth, paper, and food. ACS Nano 2018;12(3):2176–83.
[54] Ye R, James DK, Tour JM. Laser-induced graphene: from discovery to translation. Adv Mater 2019;31(1):1803621.
[55] Luong DX, Yang K, Yoon J, Singh SP, Wang T, Arnusch CJ, et al. Laser-induced graphene composites as multifunctional surfaces. ACS Nano 2019;13(2):2579–86.
[56] Groo L, Nasser J, Inman D, Sodano H. Laser induced graphene for in situ damage sensing in aramid fiber reinforced composites. Compos Sci Technol 2021;201:108541.
[57] Groo L, Nasser J, Zhang L, Steinke K, Inman D, Sodano H. Laser induced graphene in fiberglass-reinforced composites for strain and damage sensing. Compos Sci Technol 2020:108367.
[58] Nasser J, Zhang L, Sodano H. Laser induced graphene interlaminar reinforcement for tough carbon fiber/epoxy composites. Compos Sci Technol 2021;201:108493.
[59] Nasser J, Groo L, Zhang L, Sodano H. Laser induced graphene fibers for multifunctional aramid fiber reinforced composite. Carbon; 2019.
[60] Steinke K, Groo L, Sodano HA. Laser induced graphene for in-situ ballistic impact damage and delamination detection in aramid fiber reinforced composites. Compos Sci Technol 2020:108551.
[61] Solutions C. Vic-2D reference manual. 2009.
[62] Reifsnider KL. Fatigue of composite materials. Elsevier; 2012.
[63] Movahedi-Rad AV, Keller T, Vassilopoulos AP. Fatigue damage in angle-ply GFRP laminates under tension-tension fatigue. Int J Fatig 2018;109:60–9.
[64] Talreja R. Multi-scale modeling in damage mechanics of composite materials. J Mater Sci 2006;41(20):6800–12.